David Tomás Sánchez Martínez
Lourdes García Rodríguez
(coordinadores)

Proceedings of the 7th International Seminar on ORC Power Systems

Editorial Universidad de Sevilla

Proceedings of the 7th International Seminar on

ORC

Power Systems

David Tomás Sánchez Martínez
Lourdes García Rodríguez
(coordinadores)

Proceedings of the 7th International Seminar on

ORC Power Systems

(ORC2023)

4th to 6th
SEPTEMBER
SEVILLE 2023

EDITORIAL UNIVERSIDAD DE SEVILLA

Sevilla, 2024

Colección Actas
Núm.: 91

Review chairs of the 7th International Seminar on ORC Power Systems

Prof. Christoph Wieland (University of Duisburg-Essen) - *Review Chair*
Prof. Sotirios Karellas (National Technical University of Athens) - *Review Co-Chair*
Prof. Teemu Turunen-Saaresti (LUT University) - *Review Co-Chair*
Dr. Diego-César Alarcón-Padilla (Plataforma Solar de Almería - CIEMAT) - *Review Co-Chair*
Dr. Francesco Crespi (Universidad de Sevilla) - *Review Co-Chair*

c/ Porvenir, 27 - 41013 Sevilla.
Tlfs.: 954 487 447; 954 487 451; Fax: 954 487 443
Correo electrónico: info-eus@us.es
Web: https://editorial.us.es

ISBN 978-84-472-2745-7
DOI: https://dx.doi.org/10.12795/9788447227457

Diseño de cubierta y maquetación: los autores

INDEX OF CONTRIBUTIONS

SEVILLE 2023
7th International Seminar on O.R.C. Power Systems

DOI: https://dx.doi.org/10.12795/9788447227457_82

Comparison of Different Evaporator Topologies for Industrial Heat Pumps

Sanjay Vermani [1*], Nitish Anand [1], Johan Van Bael [1], Evgueni Touliankine [2], Aldo Serafino [2], Carlo De Servi [1,3]

[1] Thermal Energy Systems Group, Energy Technology Unit, Flemish Institute for Technological Research (VITO), Mol, Belgium.

[2] Enertime Courbevoie, France

[3] Propulsion & Power Group, Faculty of Aerospace Engineering, Delft University of Technology, Delft, The Netherlands.

* Corresponding Author: sanjay.vermani@vito.be

ABSTRACT

Reducing the energy consumption associated with industrial process heating is one of the crucial steps toward building a green and climate-neutral Europe, as the thermal energy demand of industry accounts for a significant portion of the total primary energy consumption and carbon emissions of this sector. In this regard, waste heat utilization using high-temperature heat pump systems is one of the most promising solutions to increase industrial energy efficiency. To efficiently recover and convert the available waste heat, the performance of the individual heat pump components, in particular the heat exchangers, is key. This paper reports a comparison between two different evaporator concepts considered for high-temperature heat pump systems, namely the shell and tube and the falling film evaporator. Four key characteristics of the two evaporator concepts are analyzed and compared: the overall heat transfer coefficient, the induced pressure losses, the footprint, and the required refrigerant charge. The results indicate that the falling film evaporator features a higher overall heat transfer coefficient and enables approximately a 77% reduction of the required working fluid charge with respect to the shell and tube evaporator.

1. INTRODUCTION

A critical milestone toward attaining climate neutrality is the decarbonization of the energy demand in industry. Currently, process heating accounts for a significant proportion of the total energy demand of the industrial sector. For example, in 2019, the share associated with process heating alone was approximately 53% (Robert et al., 2020). One of the solutions to offset this energy demand consists in recovering waste thermal energy from industrial processes.

In such a context, the exploitation of waste heat through high-temperature heat pump (HTHP) systems is recognized as one of the main options to enhance industrial energy efficiency (Kosmadakis, 2019; Arpagaus et al., 2018). However, despite the potential of the technology, the deployment of high-temperature heat pumps in industrial processes is still marginal. The reason thereof is related to several technical limitations, e.g., low thermal efficiencies, relative large footprint, and other installation requirements, which hamper the integration of new heat pump systems in existing factories (Jiang et al., 2022).

Heat exchangers are key components of this technology, as their design affect the thermodynamic, and economic performance of the heat pump. A conventional vapour compression cycle-based heat pump comprises at least two heat exchangers, namely an evaporator and a condenser. As far as the evaporator is concerned, such a component enables the heat transfer between the waste heat source and the working fluid. In large-scale industrial heat pump systems, the evaporator is often of the shell and tube type with a kettle configuration (Reay, 2002; Zohuri, 2022). The simplicity of the design and operation is obtained at the cost of a large working fluid inventory and installation footprint. A potential alternative to kettle boilers, or more in general pool-boiling heat exchangers, is the falling film evaporator with horizontal tubes. This solution offers several advantages, like reduced installation footprint and operating costs (Höfler, 2019). Those benefits arise from the higher heat transfer coefficient on the working fluid side of the heat exchanger, and the reduced amount of working fluid charge needed (Roques and Thome, 2007a). In recent years, horizontal falling film evaporators have seen successful applications in various industrial sectors, such as petrochemicals, seawater desalination and refrigeration systems (Fernández-Seara and Pardiñas, 2014).

This article reports a comparative study between a shell and tube pool-boiling type evaporator and a falling film evaporator for an industrial high-temperature heat pump. The comparison is drawn at design point conditions, with respect to key performance quantities, such as the overall heat transfer coefficient, pressure losses, installation footprint, and the required refrigerant charge. Furthermore, an off-design performance analysis was performed for the falling film evaporator. The performance of the falling film evaporator was simulated by means of a 1D steady-state model, while the commercial design software ASPEN was utilized to simulate the shell and tube evaporator (Aspentech, 2022).

2. METHODOLOGY

This section describes the modelling approach adopted for the the falling film and shell and tube evaporator models.

2.1 Falling Film Evaporator (FF)

To simulate the falling film evaporator, a steady-state lumped parameter model was developed, whose system boundaries are shown in Figure 1. The hot fluid enters the tubes from the top inlet, while the cold refrigerant is sprayed onto the tube bundle. To simplify the model, the following assumptions are made:

1. The shell-side pressure is constant.
2. Thermal losses to the environment are negligible.
3. Flow maldistribution effects due to non-uniform liquid film distribution over the tubes are neglected.

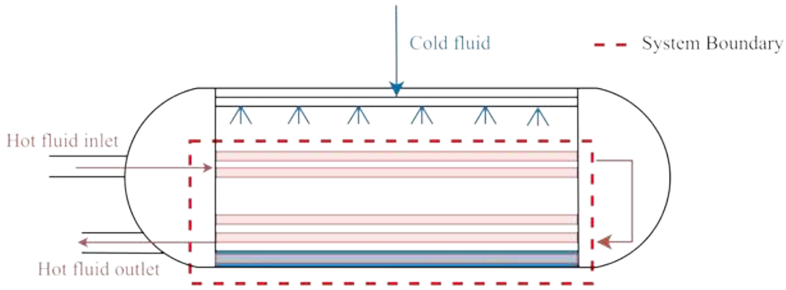

Figure 1: System boundaries of the falling film evaporator model.

To capture the variation of the mass flow rate of the liquid film from the top to the bottom rows, a tube row-wise discretization of the evaporator is implemented, as shown in Figure 2, where the index "i" and "j" refer to a given tube row and pass, respectively.

The energy balance and heat transfer rate across a tube can be expressed as

$$\dot{m}_{\text{hot, i}} c_{P,\text{hot, i}} \left(\mathrm{T}_{\text{hot in, i}} - \mathrm{T}_{\text{hot out, i}}\right) = \pi \mathrm{d}_{\text{inner}} \, L_{\text{tube}} \, h_{\text{hot, i}} \left(\mathrm{T}_{\text{hot mean, i}} - \mathrm{T}_{\text{wall inner, i}}\right), \tag{1}$$

$$\dot{m}_{\text{evap, i}} \, \Delta H_{\text{vap}} = \pi \mathrm{d}_{\text{outer}} \, L_{\text{tube}} \, h_{\text{film, i}} \left(\mathrm{T}_{\text{wall outer, i}} - \mathrm{T}_{\text{film}}\right), \tag{2}$$

$$\dot{m}_{\text{hot, i}} c_{P,\text{hot, i}} (\mathrm{T}_{\text{hot in, i}} - \mathrm{T}_{\text{hot out, i}}) = \frac{2\pi \, \lambda_{\text{wall}} \, L_{\text{tube}} \left(T_{\text{wall inner, i}} - T_{\text{wall outer, i}}\right)}{\ln\left(d_{\text{outer}}/d_{\text{inner}}\right)}, \tag{3}$$

where Equation (1) and Equation (2) express the energy balance and heat transfer rate for the hot fluid inside the tubes and the cold fluid film respectively, while Equation (3) refers to the tube wall.

Here, $\dot{m}$ is the fluid mass flow rate, c_P the specific heat capacity, T the temperature, λ the thermal conductivity, and h the heat transfer coefficient. The parameters d_{outer}, d_{inner} and L indicate the tube's outer

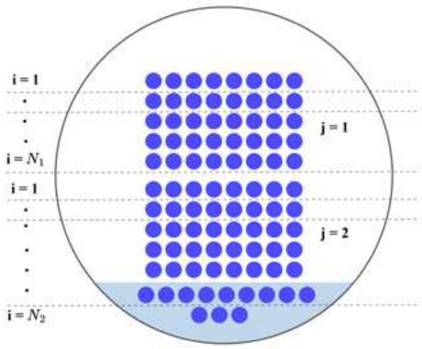

Figure 2: Discretization scheme used for the falling film evaporator model.

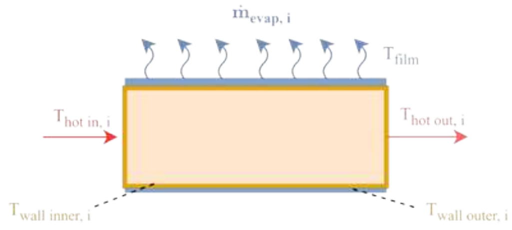

Figure 3: Schematic of the elementary volume of the discretization scheme adopted in the falling film evaporator model.

diameter, inner diameter, and length. The subscripts 'out' and 'in' refers to the inlet and outlet of an individual tube.

To estimate the convective heat transfer coefficient of the hot fluid inside the tubes (h_{hot}), the correlation proposed by Bell and Muller (2001) is used. This correlation accounts for the fluid properties and the tube characteristics and reads

$$h_{\text{hot}} = \frac{C\,\lambda_{\text{hot}}}{d_{\text{inner}}}\,\text{Re}^{0.8}\,\text{Pr}^{1/3}\left(\frac{\mu_{\text{hot}}}{\mu_{\text{wall, inner}}}\right)^{0.14}, \tag{4}$$

where Re and Pr represent the Reynolds number and Prandlt number. Besides, μ represents the dynamic viscosity of the fluid and C is a constant that varies depending on the tube type (plain or finned). In the current study, plain tubes are considered. The corresponding value of C is 0.021.

Concerning the liquid film, three main flow modes have been described in the literature, namely, droplet, column/jet, and sheet mode (Mitrovic, 1986), that may influence heat transfer. In addition, two intermediate flow modes can establish in the falling film: column-sheet and droplet-sheet, as reported by Hu and Jacobi (1996). The dependency of the heat transfer coefficient as a function of the flow mode is, to a first approximation, limited, and, at the same time, quite complex to model, as mentioned in (Roques and Thome, 2007b). Thus, in engineering practice, the heat transfer correlations account only for the onset of dryout (Yang and Wang, 2011).

Different methods have been proposed in the literature (Zhao et al., 2022; Thome, 2016) to predict the onset of dryout and the corresponding heat transfer coefficient as a function of film Reynolds number and heat flux. However, since the majority of these methods have been developed for specific fluids and are only valid for a specific range of Reynolds number and heat flux, their applicability to the evaporator of the heat pump system under investigation in this study is arguable. Therefore, three different correlations for the film heat transfer coefficient were assessed. The predictions of these correlations were compared with literature data to identify the most suitable one for the design of a falling film evaporator for the considered heat pump system (see Section 4.1).

The first method is the one developed by Shah (2021) for plain tubes, which can be, in principle, used with arbitrary fluids. Such a method is an extension of the superposition method reported by Rohsenow (1952). The other two procedures evaluated for the film heat transfer coefficient estimation were those developed by Roques and Thome (2007b) and Jin et al. (2019). As that of Shah (2021) was eventually selected for the falling film evaporator model, only this method is reported here in detail.

According to Shah (2021), the overall heat transfer coefficient during boiling in forced convection can be expressed as a linear combination of the heat transfer due to nucleate boiling and that due to forced convection. Moreover, when nucleate boiling occurs, the stirring action of the bubbles makes the transition from laminar to turbulent flow occur at low Reynolds numbers. Then, the two-phase heat transfer coefficient for the falling film can be written as

$$h_{\text{film}} = \max\left[h_{\text{c,lam}}, \left(h_{\text{nb}} + h_{\text{c,turb}}\right)\right], \tag{5}$$

where h_{nb} represents the heat transfer coefficient for the nucleate boiling regime, while $h_{\text{c,lam}}$ and $h_{\text{c,turb}}$ represent the laminar and the turbulent forced convection heat transfer coefficient, respectively.

To compute the forced convection heat transfer coefficients, the method of Shah relies on the correlations developed by Lorenz and Yung (1979) for the laminar and turbulent flow regime, which read

$$h_{\text{c,lam}} = 0.821\left(\frac{\nu_{\text{film}}^2}{g\lambda_{\text{film}}^3}\right)^{-1/3} \text{Re}_{\text{film}}^{-0.22}, \tag{6}$$

$$h_{\text{c,turb}} = 0.0038\left(\frac{\nu_{\text{film}}^2}{g\lambda_{\text{film}}^3}\right)^{-1/3} \text{Re}_{\text{film}}^{0.4}\left(\frac{\nu_{\text{film}}}{\alpha_{\text{film}}}\right)^{0.65}. \tag{7}$$

In Equation (6) and Equation (7), ν and α are the kinematic viscosity and the thermal diffusivity of the fluid, respectively. Besides, Re_{film} is defined as $\text{Re}_{\text{film}} = 4\Gamma/\mu_{\text{film}}$, where Γ is the film mass flow rate per unit length on one side of the tube.

In Equation (5), h_{nb} is estimated using the correlations developed by Mostinski (1963) and Cooper (1984). Shah (2021) recommends Mostinski's correlation for hydrocarbons and Cooper's correlation for all the other fluids. For completeness, the two correlations are reported below

$$h_{\text{nb}} = \begin{cases} \mathit{Mostinski}:\ 0.00417\, q^{0.7} p_{\text{c}}^{0.69}\left(1.8p_{\text{r}}^{0.17} + 4p_{\text{r}}^{1.2} + 10p_{\text{r}}^{10}\right), \\ \mathit{Cooper}:\ 55\, q^{0.67} M^{-0.5} p_{\text{r}}^{(0.12-0.087\ln f)}\left(-0.4343\ln p_{\text{r}}\right)^{-0.55}. \end{cases} \tag{8}$$

489

In Equation (8), q represents the heat flux, M refers to the molecular weight of the refrigerant and p refers to the fluid pressure, whereas the subscripts "r" and "c" indicate the reduced and critical pressure respectively.

In the vapour superheating region of the falling film evaporator, the main heat transfer mechanism is that of forced convection. The corresponding heat transfer coefficient and friction factor are predicted with the correlations recommended in (Verein deutscher Ingenieure, 2010, Chapter G7 and M1), assuming that the tube bundle features low-finned tubes.

Once the various heat transfer coefficients are known, the overall thermal resistance (U) across a tube wall can be computed as

$$\frac{1}{U} = \frac{1}{h_{\text{int}}}\left(\frac{d_{\text{out}}}{d_{\text{in}}}\right) + \frac{d_{\text{out}}}{2\lambda_{\text{wall}}}\left(\ln\frac{d_{\text{out}}}{d_{\text{in}}}\right) + \frac{1}{h_{\text{film}}} + \text{R}_{\text{foul}}\left(\frac{d_{\text{out}}}{d_{\text{in}}}\right), \tag{9}$$

where the reference area is the external one of the tubes. The heat flux over each tube row is evaluated assuming the log-mean temperature difference (LMTD) as the effective temperature difference between the hot and the cold fluid, namely

$$q = U\cdot\text{LMTD} = U\,\frac{\left(T_{\text{hot in, i}} - T_{\text{hot out, i}}\right)}{\ln\left(\frac{T_{\text{hot in, i}} - T_{\text{film}}}{T_{\text{hot out, i}} - T_{\text{film}}}\right)}. \tag{10}$$

Finally, the total thermal energy exchange in the evaporator is computed as

$$Q_{\text{total}} = \sum_{j=1}^{N_{\text{pass}}}\sum_{i=1}^{N_{\text{j}}} q_{(\text{j, i})}\, A_{\text{tube}}\,, \tag{11}$$

where A_{tube} refers to the outer surface area of a single tube.

The complete procedure used to design the falling film evaporator is illustrated in Figure 4. Given the process conditions, the evaporation region is designed first. Next, the number of tubes required for the vapour superheating is computed, and finally, the required shell geometry is obtained. The whole model is linked to an optimizer, as also shown in the same figure.

The target of the optimization is the minimization of the net volume of the evaporator while satisfying various design constraints, namely, the overall thermal duty and the minimum evaporated mass flow rate. The design variables are the tube length, the number of tubes in the first and second pass of the tube bundle where the evaporation occurs, as well as the number of tubes per row. All the other geometric characteristics, such as tube diameter and fin dimensions, are prescribed inputs.

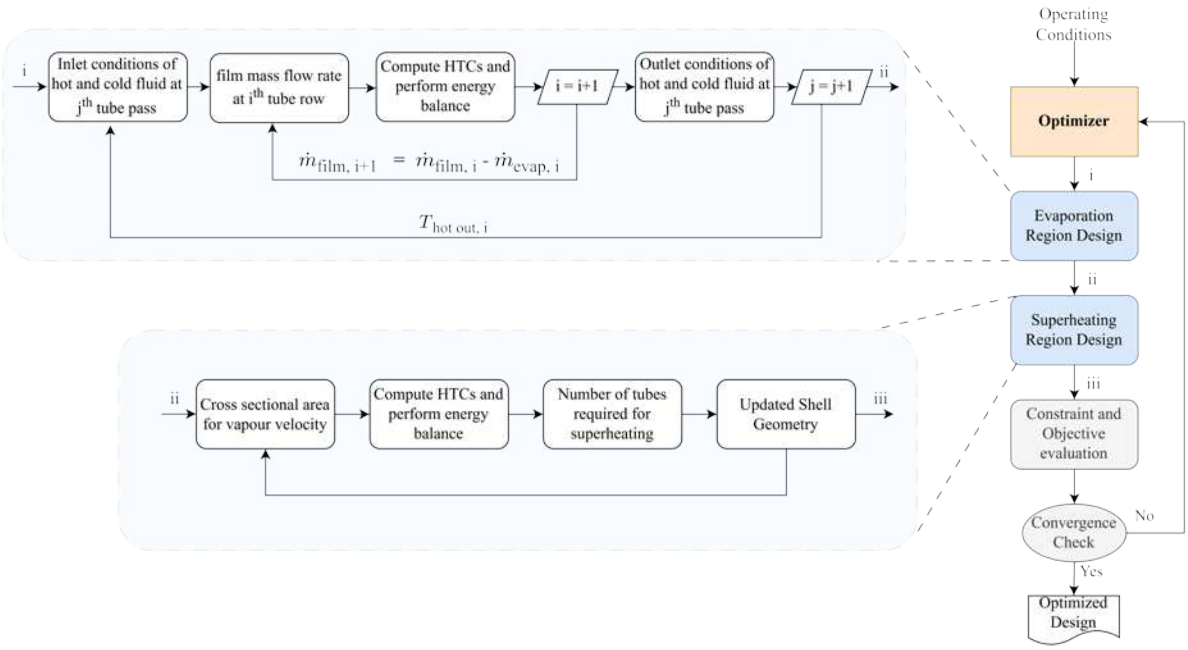

Figure 4: Falling film evaporator model structure.

490

All the fluid properties are evaluated using `REFPROP-10.0` (Lemmon et al., 2018). The Single Objective Genetic Algorithm (SOGA) is used as the optimization method, while the Latin hypercube sampling (LHS) algorithm is adopted to obtain an initial population of the solutions of SOGA, with 10 samples per design variable (Blank and Deb, 2020).

2.2 Shell and Tube Evaporator (ST)

The commercial software package `ASPEN` (Aspentech, 2022) is used to model the shell and tube pool-boiling type evaporator. This features an unbaffled tube bundle with 4 passes on the tube side and a single one on the shell side (TEMA Type: NXN).

3. CASE STUDY

The application of interest is a vapour compression cycle-based industrial high-temperature heat pump (HTHP). Figure 5 shows the schematic of the selected heat pump and Table 1 presents the associated design specifications of the evaporator. As mentioned earlier, the total shell volume was selected as the design objective to be minimized. The bounds of the design variables included in the optimization are shown in Table A1.

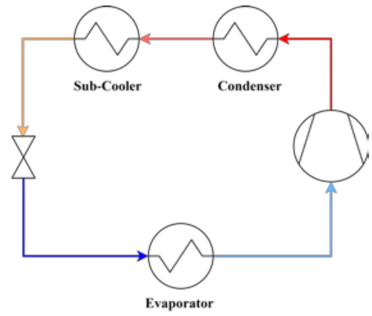

Figure 5: Selected heat pump process flow diagram.

Table 1: Evaporator design specifications for the selected heat pump test case.

	Refrigerant (R1233zdE)		Hot Source (H_2O)	
	In	Out	In	Out
Temperature [K]	340.15	355.15	365.15	345.15
Mass flow rate [kg s^{-1}]	15.44	15.44	25.0	25.0
Vapor Quality [-]	0.2715	1.0	0.0	0.0
Pressure [10^5 Pa]	4.73	-	4.0	-

4. RESULTS AND DISCUSSION

This section reports first the verification study of the developed falling film evaporator model. Subsequently, the comparison between the falling film and the shell and tube evaporator design is reported for the heat pump case under consideration.

4.1 Falling Film (FF) Model Verification

To verify the falling film evaporator model, the numerical results reported by Höfler (2019) were used as a benchmark. The author documented a 2D model of a falling film evaporator for an ORC application, though the adopted film heat transfer coefficient correlation was not mentioned. As discussed previously, the model developed in this work can make use of three different correlations to this purpose, more precisely those proposed by Roques and Thome (2007b), Jin et al. (2019), and Shah (2021).

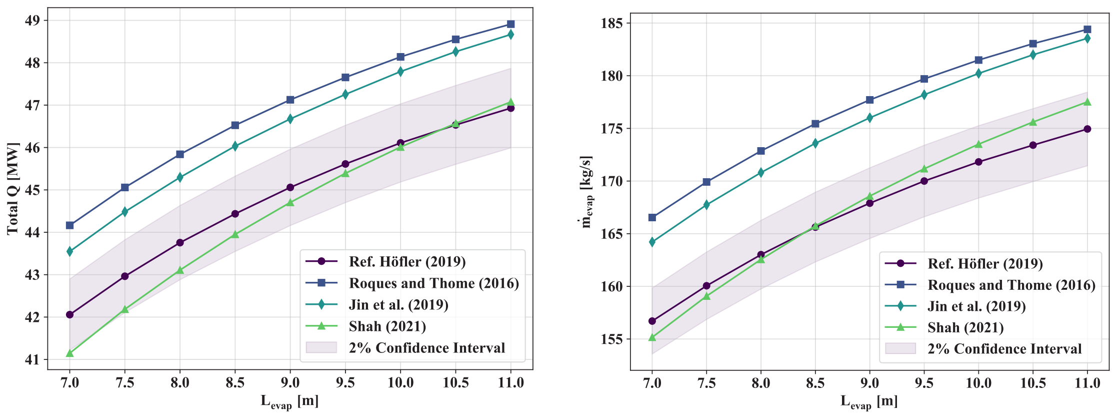

(a) Total thermal energy exchange. **(b) Evaporated fluid mass flow rate.**

Figure 6: Falling Film evaporator model verification with the data provided in Höfler (2019).

Figure 6a and Figure 6b show the comparison between the results reported by Höfler (2019) and those obtained from the model developed in this study. Notably, the overall thermal duty and the evaporated fluid mass flow rate are compared for the three different film heat transfer correlations considered in this work. It can be observed that the correlation developed by Roques and Thome (2007b) and that of Jin et al. (2019) result in a relative deviation of about ~5% with respect to the reference data. Conversely, the correlation developed by Shah (2021) show a maximum difference of ~2%. Note that the correlations of Jin et al. (2019) and Shah (2021) were derived by considering experimental data for falling films of different fluids. However, Jin et al. (2019) only considered 5 fluids and reported a high discrepancy between the predictions of the correlations and the experimental data (+/- 30%), whereas Shah (2021) considered 11 different fluids and reported a higher accuracy of the developed correlation (+/- 20% of deviation with respect to the experimental data). Based on this consideration and the better match with the data in Höfler (2019), the correlation of Shah (2021) was, thus, selected for the design of the falling film evaporator in this study.

4.2 On-design Results

Both the falling film (FF) and the shell and tube (ST) evaporator were designed for the process specifications reported in Table 1. Table 2 compares the corresponding characteristics of the two heat exchangers, where ϵ represents the relative difference of a specific design characteristic (x) with respect to the shell and tube evaporator design. The FF evaporator features plain tubes in the evaporating region and finned tubes in the superheating part. For the ST evaporator, finned tubes were considered for the whole tube bundle. The main geometric parameters of the considered plain and finned tubes are presented in Table A2.

Table 2: Main characteristics of the falling film and shell and tube evaporators at design conditions.

Parameter	Unit	Shell and Tube	Falling Film	ϵ [%]
Total Cold Fluid Evaporated	$kg\ s^{-1}$	11.25	11.25	0.0
No. of Tubes for Evaporation	-	305	120	−60.7
No. of Tubes for Superheating	-	202	148	−26.7
Tube Length	m	5.9	5.79	−1.9
Shell Outer Diameter	m	0.65	0.61	−6.2
Total Shell Volume	m^3	1.97	1.67	−15.2
Average U	$W\ m^{-2}\ K^{-1}$	555.1	1455.8	162.3
Liquid Refrigerant Inventory	kg	1590.7	361	−77.3
Pressure Drop Hot Fluid	kPa	67.1	21.5	−67.9

The overall heat transfer coefficient for the FF evaporator is 2.6 times higher than that of the ST evaporator. As a result, the heat transfer area required is smaller for the FF heat exchanger, and the number of tubes in the evaporating region is more than halved as compared to the ST evaporator. The latter features four tube passes, whereas the FF evaporator three tube passes, one for superheating and two for evaporation. This difference in the pass configuration, in combination with shorter tubes, results in a three-time lower pressure drop in the hot fluid inside the tubes in the case of the FF evaporator as compared to the ST one. 492

Another significant difference between the two heat exchanger types is the required cold fluid inventory in operation. This quantity was estimated by evaluating the liquid level in the shell, given the number of submerged tubes, and the corresponding volume. Notice that there is no accumulation of working fluid in the FF evaporator during operation. This heat exchanger has a limited number of fully submerged tubes, whereas in the ST evaporator 60 % of the tubes are fully submerged. Therefore, the required liquid refrigerant mass in the FF heat exchanger during operation is ~77% lower than in the ST evaporator.

Figure 7a and Figure 7b shows the cross-sectional view of the ST and FF evaporators, respectively. In the case of the FF evaporator (see Figure 7b), a qualitative representation of the film liquid distributor over the tubes is also included. Due to the high degree of superheating targeted in the design, a large number of tubes are required in both evaporators to reach this vapour condition. In addition, a different tube arrangement is adopted in the main two zones of the FF evaporator: the tube bundle where the vapour is superheated features a staggered arrangement, while that where the fluid evaporates an inline configuration with a much lower number of tubes per unit volume. Thus, a more compact tube arrangement is achieved in the ST evaporator. It results that the shell diameter of the two heat exchangers is similar, in spite of the lower required heat transfer area in the case of the FF topology.

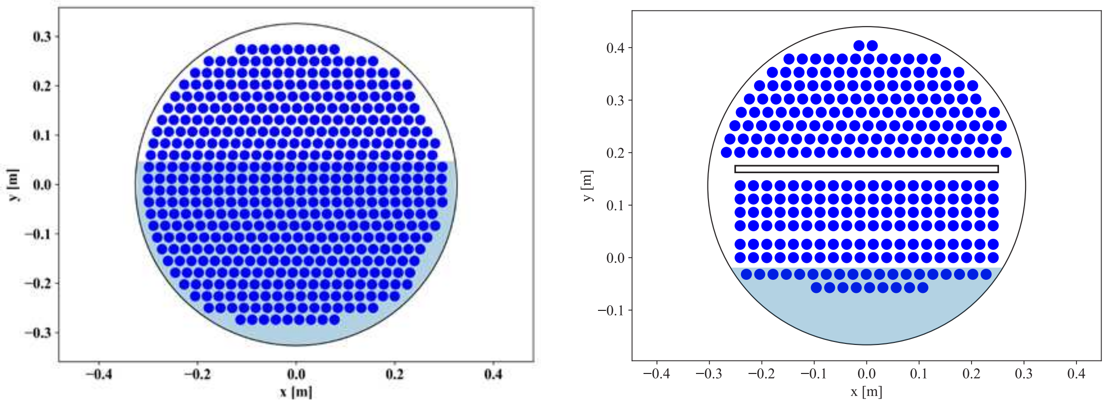

(a) Shell and Tube **(b) Falling Film**

Figure 7: Cross-sectional view of the tube bundle for the two evaporator types.

4.3 Falling Film Evaporator Off-design Performance

This section describes how the thermal performance of the FF evaporator, with the geometry specified in Table 2, varies as a function of the injected working fluid mass flow rate. In particular, Figure 8 shows the corresponding trend in the evaporator thermal duty and the non-evaporated fluid mass flow rate: the higher the injected mass flow rate, the greater the thermal duty and the amount of evaporated working fluid. The increase is, however, limited. The thermal duty augments by less than 1% with respect to the nominal conditions. At the same time, the difference between the injected mass flow rate and the evaporated one increases, leading to a rise in the liquid level in the shell over time. System operation becomes thus feasible only if the evaporator is equipped with a recirculation pump. It is worth also noting that these trends pertain to an optimal FF evaporator design obtained assuming no fluid recirculation. A better peformance may be achieved if the evaporator design is optimized for larger film flows than the targeted evaporating mass flow rate.

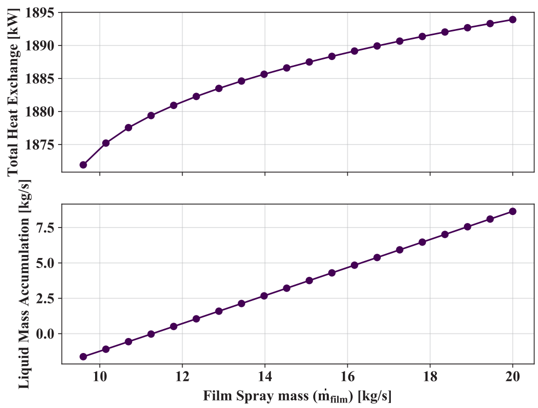

Figure 8: Falling film evaporator performance with film spray mass flow rate (top: thermal duty, bottom: liquid accumulation).

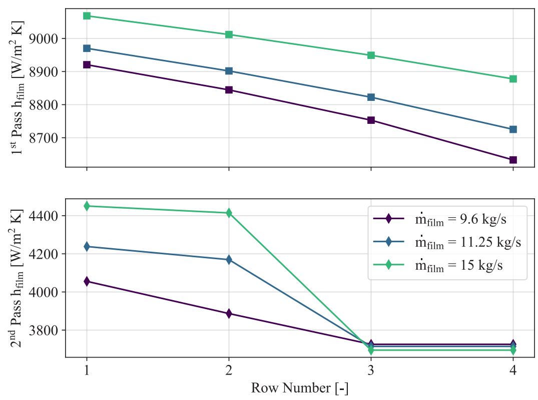

Figure 9: Row-wise heat transfer coefficient variation with film spray mass flow rate (top: first tube pass, bottom: second tube pass).

Figure 9 illustrates the variation of the film heat transfer coefficient along the tube rows of the two passes in the evaporation region as a function of the film mass flow rate. The heat transfer coefficient in the second pass is consistently lower than that in the first pass, regardless of the sprayed mass flow rate. This phenomenon can be attributed to the decrease in the total liquid mass from the top to the bottom of the evaporator. Additionally, the temperature of the hot fluid inside the tubes decreases as it moves downwards. Thus, a higher temperature difference is established at the top of the heat exchanger than at the bottom. Notice also that the last two rows of the second pass are fully submerged by the liquid.

If the local film mass flow rate on the tube surface is insufficient and the corresponding tube wall temperature is high enough, a local dryout may occur. This results in a smaller effective wetted area on the tube, leading to a lower effective heat transfer coefficient. This effect becomes more prominent at low film mass flow rates. One potential strategy to prevent these conditions is to implement a control loop over the working fluid feed pump, thereby ensuring a proper wetting of the tubes. However, this strategy, again, entails the use of a recirculation pump to maintain a constant liquid level in the shell (Höfler, 2019).

5. CONCLUSIONS

This study compares two evaporator concepts, namely the falling film and the shell and tube, for an industrial high-temperature heat pump application. A 1D model of the falling film evaporator was developed and verified by comparing its predictions against reference data reported in the literature for a test case similar to that investigated in this paper. The shell and tube evaporator is of the pool-boiling type, features a tube bundle with four passes on the hot side, and its design was performed using the commercial tool ASPEN. Based on the results of this study, the following conclusions can be drawn

1. The falling film evaporator features a 2.6 times higher overall heat transfer coefficient with respect to the shell and tube heat exchanger.
2. A fluid inventory reduction of around 77% is achieved by means of the falling film evaporator due to the lower number of submerged tubes. In addition, the falling film evaporator allows for about a 15% reduction in total component volume, as compared to the standard shell and tube evaporator.
3. For high degrees of superheating, the required number of tubes tends to be large, dictating the overall shell size for the case of the falling film evaporator. Therefore, it is expected that the smaller the degree of superheating, the more compact the falling film evaporator.
4. The heat transfer in the the falling film evaporator can be further enhanced increasing the injected liquid mass flow rate. This can be especially useful to prevent the occurrence of dryout in the tube rows at the bottom of the evaporator. This solution entails a higher system complexity, as a recirculation pump would be necessary to maintain a constant liquid level in the evaporator.

Future work will focus on comparying additional heat exchanger types, such as plate and shell-and-plate evaporators, to identify the most suitable heat exchanger topologies for high-temperature heat pumps.

ACKNOWLEDGEMENTS

This work was conducted within the PUSH2HEAT project, which received funding from the European Union's Horizon Europe research and innovation programme under grant agreement No.101069689.

REFERENCES

Arpagaus, C., Bless, F., Uhlmann, M., Schiffmann, J., and Bertsch, S. (2018). High Temperature Heat Pumps: Market Overview, State of the Art, Research Status, Refrigerants, and Application Potentials. *Energy*, 152:985–1010.

Aspentech (2022). Aspen v14. https://www.aspentech.com/en.

Bell, K. J. and Muller, A. C. (2001). *Wolverine Engineering Data Book II*. Wolverine Tube Inc.

Blank, J. and Deb, K. (2020). pymoo: Multi-objective Optimization in Python. *IEEE Access*, 8:89497–89509.

Cooper, M. G. (1984). Heat Flow Rates in Saturated Nucleate Pool Boiling - A Wide-Ranging Examination Using Reduced Properties. *Advances in Heat Transfer*, 16:157–239.

Fernández-Seara, J. and Pardiñas, A. A. (2014). Refrigerant Falling Film Evaporation Review: Description, Fluid Dynamics and Heat Transfer. *Applied Thermal Engineering*, 64(1):155–171.

Hu, X. and Jacobi, A. M. (1996). The Intertube Falling Film, Part 1: Flow Characteristics, Mode Transitions and Hysteresis. *Journal of Heat Transfer*, 118:616–625.

Höfler, M. (2019). *Theoretical Evaluation of Falling Film Evaporation for Organic Rankine Cycle Process*. PhD thesis, Institude of Heat and Mass Transfer RWTH Aachen, Aachen.

Jiang, J., Hu, B., Wang, R., Deng, N., Cao, F., and Wang, C.-C. (2022). A Review and Perspective on Industry High-Temperature Heat Pumps. *Renewable and Sustainable Energy Reviews*, 161:112106.

Jin, P. H., Zhang, Z., Mostafa, I., Zhao, C. Y., Ji, W. T., and Tao, W. Q. (2019). Heat Transfer Correlations of Refrigerant Falling Film Evaporation on a Single Horizontal Smooth Tube. *International Journal of Heat and Mass Transfer*, 133:96–106.

Kosmadakis, G. (2019). Estimating the Potential of Industrial (High-Temperature) Heat Pumps for Exploiting Waste Heat in EU Industries. *Applied Thermal Engineering*, 156:287–298.

Lemmon, E. W., Bell, I. H., Huber, M. L., and McLinden, M. O. (2018). NIST Standard Reference Database 23: Reference Fluid Thermodynamic and Transport Properties-REFPROP, Version 10.0, National Institute of Standards and Technology.

Lorenz, J. J. and Yung, D. (1979). A Note on Combined Boiling and Evaporation of Liquid Films on Horizontal Tubes. *Journal of Heat Transfer*, 101:178–180.

Mitrovic, J. (1986). Influence of Tube Spacing and Flow Rate on Heat Transfer from a Horizontal Tube to a Falling Liquid Film. *Proceedings of the Eighth International Heat Transfer Conference*, 4:1949–1956.

Mostinski, I. L. (1963). Application of the Rule of Corresponding States for Calculation of Heat Transfer and Critical Heat Flux. *Teploenergetika*, 4:66–71.

Reay, D. A. (2002). Compact Heat Exchangers, Enhancement and Heat Pumps. *International Journal of Refrigeration*, 25(4):460–470.

Robert, d. B., Marina, A., Zühlsdorf, B., Arpagaus, C., Bantle, M., Wilk, V., Elmegaard, B., Corberán, J., and Benson, J. (2020). Strengthening industrial heat pump innovation: Decarbonizing industrial heat.

Rohsenow, W. M. (1952). A Method of Correlating Heat-Transfer Data for Surface Boiling of Liquids. *Trans. ASME*, 74:969–975.

Roques, J. F. and Thome, J. R. (2007a). Falling Films on Arrays of Horizontal Tubes with R-134a, Part I: Boiling Heat Transfer Results for Four Types of Tubes. *Heat Transfer Engineering*, 28(5):398–414.

Roques, J. F. and Thome, J. R. (2007b). Falling Films on Arrays of Horizontal Tubes with R-134a, Part II: Flow Visualization, Onset of Dryout, and Heat Transfer Predictions. *Heat Transfer Engineering*, 28:415–434. 495

Shah, M. M. (2021). A General Correlation for Heat Transfer during Evaporation of Falling Films on Single Horizontal Plain Tubes. *International Journal of Refrigeration*, 130:424–433.

Thome, J. R. (2016). *The Heat Transfer Data Book III: Enhanced Heat Transfer Design Methods for Tubular Heat Exchangers*. Publico Publications.

Verein deutscher Ingenieure (2010). *VDI Heat Atlas*. Springer.

Yang, L. and Wang, W. (2011). The Heat Transfer Performance of Horizontal Tube Bundles in Large Falling Film Evaporators. *International Journal of Refrigeration*, 34:303–316.

Zhao, C.-Y., Qi, D., Ji, W.-T., Jin, P.-H., and Tao, W.-Q. (2022). A Comprehensive Review on Computational Studies of Falling Film Hydrodynamics and Heat Transfer on the Horizontal Tube and Tube Bundle. *Applied Thermal Engineering*, 202:117869.

Zohuri, B. (2022). *Compact Heat Exchangers*. Springer.

A. APPENDIX

Table A1: Bounds considered for the design variables of the falling film evaporator

Design Variable	Bounds
Number of tube rows (1st pass)	[2, 25]
Number of tube rows (2nd pass)	[2, 25]
Number of tubes per row	[2, 20]
Length of tube	[0.5, 6.0]

Table A2: Geometric characteristics of the tubes.

Parameter	Unit	Plain Tube	Finned Tube
d_{outer}	mm	19.05	19.05
d_{inner}	mm	17.78	12.58
d_{root}	mm	-	15.88
Fin height	mm	-	1.588
Fin thickness	mm	-	0.4
Fin pitch	mm	-	0.9775

This book contains the compilation of works contributed to the *7th International Seminar on Organic Rankine Cycle Power Systems* (ORC 2023), held in Seville between the 4th and 6th of September 2023. The event was hosted by Universidad de Sevilla on behalf of the Knowledge Centre on Organic Rankine Cycle Technology (KCORC), incorporated in The Netherlands.

The ORC conference, organized biennially, stems as the only conference that is specific to ORC technology, therefore gathering a diverse community whose affiliation spans across all the interested stakeholders, not only in this particular technology but also and in a broader context, in the energy transition. Original equipment manufacturers, professional associations, end-users, investors, policy makers, academics, scientists feel at home at ORC 2023.

The almost 100 proceedings in this book cover a wide variety of topics, from fundamentals to system integration through component design, accounting for thermodynamic performance as well as component design. In addition to this, and as a new track in 2023, works on heat pump technology were also accepted in order to raise awareness of the strong ties between both technologies, specifically in energy storage applications.

This book provides an excellent overview of the current maturity of power systems based on Organic Rankine Cycle technology for applications as diverse as geothermal and waste heat recovery in industry or downstream of other prime movers (e.g., marine applications). It is also an excellent source of information to understand the current challenges faced by the technology, stemming from a very competitive market and increasingly stringent environmental regulations.

The organizers of ORC 2023 hope that the reader finds this work as exciting as the attendees to the conference and, maybe, make the decision to join the 8th edition to the conference in 2025.

KCORC
KNOWLEDGE CENTER
ORGANIC RANKINE CYCLE

eus EDITORIAL
UNIVERSIDAD DE SEVILLA